Journal of Thermal Biology 115 (2023) 103624

Contents lists available at ScienceDirect

Journal of Thermal Biology

journal homepage: www.elsevier.com/locate/jtherbio

Denatured collagen inhibits neuroblastoma tumor-sphere migration and growth via the LOX/LOXL2 – FAK signaling pathway

Chi-Bao Bui [a,b,f,1], Kha Dong To [b,e,f,1], Diem My Vu [c], Quynh-Giang Nguyen [b,f], Hiep Thi Nguyen [d], Si-Bao Nguyen [b,f,*]

[a] Unit of Molecular Biology, City Children's Hospital, Ho Chi Minh City, Vietnam
[b] School of Medicine, Ho Chi Minh City, Vietnam
[c] Center for Molecular Biomedicine, University of Medicine and Pharmacy at Ho Chi Minh City, Vietnam
[d] School of Biomedical Engineering, International University, Ho Chi Minh City, Vietnam
[e] University College London, London, United Kingdom
[f] Vietnam National University, Ho Chi Minh City, Vietnam

ARTICLE INFO

Keywords:
Collagen
Thermal ablation
Neuroblastoma
LOX/LOXL2
FAK
Epithelial-mesenchymal transition

ABSTRACT

A complex interplay exists within the tumor microenvironment and extracellular matrix, which could contribute to solid tumor progression. Collagen, a major component of the extracellular matrix, may correlate with cancer prognosis. While thermal ablation has shown promise as a minimally invasive treatment of solid tumors, its impact on collagen is still unknown. In this study, we demonstrate that thermal ablation, but not cryo-ablation, induces irreversible collagen denaturation in a neuroblastoma sphere model. Prolonged collagen denaturation resulted in a significant reduction in sphere stiffness, migration, and proliferation, and an increase in apoptosis. Mechanistic analysis revealed that collagen denaturation inhibited collagen cross-linking, reduced extracellular LOX/LOXL2 expression, and resulted in decreased phosphorylation of FAK. Downstream of FAK, we observed reduced epithelial to mesenchymal transition, attenuated CDC42 expression, and decreased migration. Collectively, these results suggest that denatured collagen presents a novel target for modulating the tumor microenvironment and treating solid cancers via the LOX1/LOXL2-FAK signaling pathway.

1. Introduction

Neuroblastoma (NB) is one of the most aggressive solid tumors in pediatric oncology (Ahmed et al., 2017). Multi-modal therapeutic approaches to NB include resection, intensive chemotherapy, radiation, immunotherapy and 13-cis-retinoic acid treatment (Pinto et al., 2015). Nevertheless, overall survival remains low, and disease recurrence common, with most patients developing metastases (Franco-Luzon et al., 2020). Moreover, NB cancer driving genes exhibit low frequency mutation (Franco-Luzon et al., 2020) indicating that treatment should rely on reprogramming of cell fates and consider the complexity of cellular interactions. New approaches should focus on the heterogeneity of the local tumor microenvironment (TME) where the extracellular matrix (ECM) may determine the heterogeneity of cancer cells.

The TME is comprised of tumor cells, resident cells (e.g. endothelial cells and fibroblasts), infiltrating cells (e.g. lymphocytes, macrophages) and the ECM (e.g. collagen, fibronectin) (Hanahan and Weinberg, 2011). Targeting TME treatment is considered a preferred method than conventional therapies by its ability to activate antitumor immunity and boost the efficacy of immune-targeted agents in neuroblastoma (Binnewies et al., 2018; Joshi, 2020). Thermal ablation is a newer modality which has potential advantages over TME by selectively inducing cancer cell death and activating a robust T cell-dependent antitumor immunity (Brock et al., 2020; Ringel-Scaia et al., 2019). It has recently been tested in clinical trials for treatment of hepatocellular carcinoma and renal-cell carcinoma (Pavlovich et al., 2002; Rhim et al., 2003; Takaki et al., 2017). This therapy can also be combined with advanced ultrasound imaging to improve treatment of hepatocellular carcinoma with poor surgical outcomes, and ultrasound-guided percutaneous liver resections in recurrent pediatric hepatoblastoma (Liu et al., 2015). Thermal ablation can achieve excellent, and comparable, results to surgical resection and has the advantage of minimal invasiveness with more selective cell

* Corresponding author.
E-mail address: drbaosinguyen@gmail.com (S.-B. Nguyen).
[1] These authors contributed equally to this work.

https://doi.org/10.1016/j.jtherbio.2023.103624
Received 13 June 2022; Received in revised form 16 April 2023; Accepted 11 June 2023
Available online 29 June 2023

targeting. However, the mechanism of thermal ablation therapy (Chu and Dupuy, 2014) and specifically how it impacts cellular necrosis, apoptosis and the ECM remains unclear. The ECM creates scaffolding support for its cellular constituents and plays an important role in development and cancer progression (Lu et al., 2012).Native collagen forms triple helices to serve as a basic ECM that interacts with tumor, host and other biomolecules (Xu et al., 2019).Numerous studies have investigated collagen levels and structure in various tissues, revealing that elevated levels of collagen IV in serum may serve as a prognostic marker for primary breast cancer (Mazouni et al., 2008). Additionally, high mRNA expression of COL1A1 and COL1A2 has been associated with poor progression-free survival and overall survival in cancer patients (Brooks et al., 2016). A recent report has revealed the expression of 28 collagen members in the neuroblastoma microenvironment, with a notable COL11A1 signature at the tumor-stroma boundary that supports the potential novel therapeutic intervention through collagen remodeling (Truong et al., 2022). Heating and denaturation of collagen fibrils triggers a "zipper" type dissociation with breakdown of cross-linkages dependent on glycosylation of lysine and hydroxylysine residues and di-sulphide covalent bonds (Miles and Ghelashvili, 1999; Ricard-Blum, 2011). Such alterations in collagen structure were visualized the use of mimetic peptides CHP-targeted triple-helix hybridization (Li et al., 2012) that could address the collagen transformation induced by various chemical and physical sources such as radiation, microwave, detergents (Xu et al., 2019). Herein we aim to investigate the effects of thermal ablation therapy on collagen structure and the proliferation, migration, stiffness and apoptosis of NB cancer using an in vitro tumor-sphere model to mimic the TME.

2. Material and methods

2.1. NB sphere culture

Cell lines SK-N-DZ and SK-N-AS were kindly obtained from the Akira Nakagawara's lab. These cells were maintained in complete medium DMEM (Gibco, USA), supplemented with 10% fetal bovine serum (Gibco) and 1% antibiotic-antimycotic (Gibco) at 5% CO_2 and 37 °C. NB sphere-formation was achieved by a previously published method (Izumi and Kaneko, 2014). Briefly, 1×10^4 cells were plated on Ultra-low cluster 6-well-dishes (Corning, USA) in 1:1 mixture of DMEM-F12 medium (Wako, USA) containing 1% antibiotic-antimycotic (Gibco), 2% B27 supplement (Invitrogen, USA), 1% N-2 supplement (Wako), 25 ng/mL epidermal growth factor (EGF; Wako), and 25 ng/mL fibroblast growth factor (FGF; Wako). 50% medium was replaced with fresh medium weekly. Established sphere-forming cells were counted and measured under an inverted microscope (Nikon TE-2000) at day 7, 10 and 14.

2.2. Thermal or cryo-ablation

At day 14 of culture, NB sphere-forming cells with a diameter of 30–40 μm diameter were transferred onto a slide and subjected to a fiber-coupled diode laser (Fitel FOL1425RUZ-317, 1480 nm wavelength). The beam was directed through an objective lens (Nikon, Japan), and focused onto spheres. Pulses were generated by a laser source (Opto Power OPC-PS03-A, 500 kHz) and a specified electrode probe with a diameter of 3 mm was used to raise the temperature of the spheres to a range of 45–80 °C for a duration of 30 min. Additionally, Cryo-ablation was carried out using a cooled metal disc Cryopen (Cryopen CT-2000) and suggestive 3 mm probe to reduce the temperature of the spheres to a range of −20 to −400 °C for a duration of 30 min.

2.3. Sphere stiffness and migration assay

Sphere stiffness was assessed by atomic force microscopy (AFM; Park Systems, Korea) under the manufacturer instructions and following previously published protocols (Roduit et al., 2009). Briefly, the sphere cell culture dish was placed on the AFM cantilever with the laser beam focused at 5 μm, and indenting force rate set to 1–10 μm/s. Five spheres per condition were measured. The collective indenting force was predicted following the Hertz model in MATLAB (USA). To initiate the migration assay, flat-bottomed 96-well plates (Corning Life Sciences, Vietnam) were coated with 0.1 % (v/v) gelatin (Sigma-Aldrich, Vietnam) using PBS for 1 h at 37 °C. Afterwards, 200 μl of culture medium supplemented with 2 % (v/v) FCS was added to each well. In wells containing 3-day SK-N-DZ spheroids, 100 μl of medium was removed, and the remaining medium along with the spheroids was transferred to a prepared migration, resulting in a final volume of 300 μl. The spheroids were allowed to adhere, and images were captured at 0 and 48 h using an inverted microscope. The effects of thermal treatment were then analyzed by measuring the area covered by 200 migrating spheroids per test, with data normalized to the initial size of each spheroid at 0 h.

2.4. Immunofluorescence staining

Sphere-forming cells were fixed with 4% paraformaldehyde (PFA; Sigma, USA), permeabilised with 0.5% Triton X-100 in phosphate-buffered saline (PBS; Gibco) and blocked with 3% bovine serum albumin (BSA; Gibco) for 30 min at room temperature before incubation with appropriate primary antibodies (S1 Table). Native collagen was detected by anti-collagen I (Abcam, USA) and denatured collagen by anti-5-FAM conjugate collagen hybridizing peptide (F–CHP; 3Helix, USA) (Zitnay et al., 2017). Proliferation and apoptosis were detected by anti-Ki67 (Thermo Fisher) and anti-cleavage-caspase 3 (Cell Signaling), respectively. After washing, cells were incubated with Alexa Fluor 488-conjugated secondary antibody (Thermo Fisher, USA) or Alexa Fluor 546-conjugated secondary antibody (Thermo Fisher). Prolong Gold antifade mounting reagent with DAPI and coverslip were applied in the final step. Image fluorescent signals were assessed by Olympus FluoView™ FV1000 (Biotek, USA) and captured using a Pannoramic MIDI scanner (3DHISTECH Ltd). Each sample was scored and evaluated independently by two pathologists. Sinicrope scoring method was previously used to analyze intensities of the immunofluorescent staining and the proportion of nucleus stained with DAPI (Bui et al., 2019).

2.5. Quantitative RT-PCR

Total RNA was extracted from sphere NB cell lines using the RNeasy Mini Kit (Qiagen, USA). RNA concentration and purity were estimated from optical density at 260 and 280 nm, respectively. One microgram of RNA was reverse-transcribed to cDNA using the PrimeScript RT reagent Kit (Takara, Japan) following manufacturer's instructions. qPCR was performed in triplicate in a 10 μL reaction mixture containing 5 μL SYBR Green Master Mix (Thermo Fisher Scientific, USA), 0.5 μM each of forward and reverse primers and 10 ng cDNA. The LOX, LOXL1, LOXL2, LOXL3, LOXL4, and GAPDH transcriptional levels were determined using specific primers (S2 Table). Relative quantification was carried out by $2^{-\Delta\Delta Ct}$ method after normalizing to an endogenous reference gene GAPDH. Statistical analysis of gene expression in clinical samples was conducted by using Wilcoxon two-sample test.

2.6. Immunoblotting and immunoprecipitation

For total protein extraction, cells were lysed in radioimmunoprecipitation assay buffer (10 mM Tris-HCl; pH 7.4, 150 mM NaCl, 1 mM EDTA, 1% [w/v] sodium deoxycholate, 0.1% [w/v] SDS, and 1% [v/v] NP–40) and complete protease inhibitor cocktail (Sigma) for 30 min at 4 °C. Protein extracts were quantified by Bradford assay and 30 μg/sample separated by gradient SDS gel electrophoresis before blotting onto nitrocellulose membranes (Immobilon, Sigma). Membranes were blocked with 5% non-fat dried milk powder for 30 min. Protein expression was detected using the antibodies in S1 Table. FAK

inhibitor PF562271 (Medkoo Bioscience, USA) was used as per a previously published report (Megison et al., 2013). For co-immunoprecipitation studies, cells and media were lysed in buffer A (10 mM HEPES, pH 7.9, 10 mM KCl, 0.1 mM EDTA, 1 mM DTT [dithiothreitol], 0.5% NP-40, and protease inhibitors) and incubated for 15 min on ice. Each extract was incubated with anti-LOX, or anti-LOXL2 (Abcam) and anti-COL1 (Abcam; S1 Table), immobilized on protein A or G-Sepharose (Amersham, Merck, USA), and incubated for 2 h at 4 °C. After washing with lysis buffer, immunoprecipitates were collected by centrifugation and proteins were boiled in Laemmli buffer. After centrifugation, supernatants were subjected to casting gradient 7.5–10.5% gel SDS-PAGE and transferred to PVDF membranes. Immunoreactive bands were visualized by enhanced chemiluminescence (ECL). ECL signals were detected using myECL imager (Thermo Fisher Scientific). Densitometry analysis was analysed by ImageJ. Each blot was representative of two or three independent experiments.

2.7. Quantitative LOXL2 activity

NB cell lines (SK–N-DZ and SK-N-AS) subject to thermal ablation, or hypoxia induction using hypoxia chambers (Coylab), were assessed for LOXL2 activity as previously described (Okada et al., 2018). LOXL2 assays were assessed by coupling horseradish peroxidase activity to LOXL2 relative fluorescent units. All experiments were performed at least three times under each condition and results reported as average values of relative LOXL2 activity.

2.8. Statistical analysis

Data visualization of subgroup tests and correlations were performed using Excel, SPSS 17.0 software (Chicago, IL) and GraphPad Prism V6.01 (GraphPad Software Inc). Other values were expressed as mean ± SEM, and statistical analyses were performed using one way analysis of variance (ANOVA) followed by Tukey posthoc analysis. $P < 0.05$ was deemed to be statistically significant.

3. Results

3.1. Effect of thermal ablation and cryo-ablation on collagen denaturation in sphere-forming NB cells

Sphere-forming SK-N-DZ cells were used to determine whether thermo- or cryo-ablation methods could induce collagen denaturation (dCol). We used a CHP-targeted triple-helix hybridization probe to identify dCol and the optimal conditions to induce irreversible collagen denaturation in the NB sphere model. Thermal ablation resulted in collagen denaturation as demonstrated by the presence of Fab-CHP staining and absence of anti-COL1 staining in contrast with control cells (Fig. 1A and B; $P < 0.001$). Conversely, cryo-ablation did not result in dCol as demonstrated by a lack of Fab-CHP staining, and comparable anti-COL1 staining in treated and control cells (Fig. 1A and B). Thermal ablation led to a decrease in sphere stiffness compared to control cells while cryo-ablation had no effect on sphere stiffness (Fig. 1C; $P < 0.05$). Spheres subjected to thermal ablation were assessed for 72 h to assess stability of collagen denaturation and stiffness (Fig. 1D–F). dCol and stiffness remained stable at 24 h, 48 h and 72 h post-thermal ablation (Fig. 1D–F). Thermal ablation treatment of spheres led to increased Fab-CHP expression and decreased Collagen type 1 and type IV expression in comparison to the control group demonstrating dCol (Fig. 1G). In contrast, cryo-ablation treatment had no effect on expression of F–CHP, Collagen type 1 or collagen type IV comparison to the control group (Fig. 1G).

3.2. Collagen denaturation affects proliferation, apoptosis, stiffness and migration of sphere-forming NB cells

NB sphere numbers were significantly decreased from the primary to secondary passages of cells in control conditions and also following formal ablation (Fig. 2A; $P < 0.01$). Thermal ablation led to a 2.8 fold-significant reduction in proliferation as demonstrated by lower Ki67 expression (Fig. 2B; $P < 0.01$), and significantly increased levels of apoptosis as shown by a 3.1-fold increase in cleaved-Caspase 3 (Fig. 2B; $P < 0.05$). The 3D-migration assays demonstrated a decreased spread-out process as single cell migration at 48 hours in the thermal ablation group compared to the control group(Fig. 2C; $P < 0.001$). Furthermore, there was significantly decreased CXCR4 expression, , a marker associated with NB migration at the 48 h timepoint in the thermal ablation group compared with the control group (Fig. 2D). These results indicate that thermal ablation, and resultant collagen denaturation leads to decreased proliferation and migration, and increased apoptosis, in sphere-forming NB cells.

3.3. Effect of dCol on LOX/LOXL2 crosslinking of type I collagen in sphere-forming NB cells

We next evaluated the mechanistic impact of dCol on collagen cross-linking in the ECM. Collagen cross-linking was assessed by measuring expression of lysyl oxidase (LOX), and Lysyl oxidase like-1 to 4 (LOXL 1–4). qRT-PCR analysis revealed significant reduction of LOX and LOXL2 mRNA levels in thermal ablation treated sphere-forming NB cells (Fig. 3A). LOXL2 activity, induced by hypoxia and determined by ELISA, was also significantly attenuated following thermal ablation compared with the control group (Fig. 3B). Finally, we conducted co-immunoprecipitation of two prominent expressions LOX and LOXL2 with the type I Collagen. We demonstrated that LOX and LOXL2 specifically precipitated COL1 from the lysate of control NB cells but exhibited impaired ability to bind to dCol following thermal ablation treatment (Fig. 3C). Altogether, these data show that thermal ablation treatment causes a down regulation of LOX and LOXL2 and that dCol is not sufficient for cross-linking of LOX/LOL2.

3.4. Changes in LOX/LOXL2 and dCol affects FAK signaling with subsequent effects on migration and EMT

LOX and LOXL2 have previously been implicated in activation of the FAK (focal adhesion kinase)-signaling pathway (Barker et al., 2013) and EMT (de Jong et al., 2019). The loss of collagen cross linking with LOX and LOXL2 following thermal ablation treatment prompted us to explore whether these changes affect downstream FAK signaling and EMT. As shown in Fig. 4A, dCol does not change the expression of FAK but attenuates FAK (Tyr397) phosphorylation. Furthermore, dCol leads to a reduction in expression of the downstream molecule CDC42 following thermal ablation treatment of sphere-forming NB cells. dCol increases E-Cadherin expression but decreases N-Cadherin and Vimentin expression after thermal ablation treatment (Fig. 4B). We further examined whether EMT is downstream of FAK signaling pathway. By using the selective inhibitor of FAK (PF562271), we found that PF562271 also reduced N-Cadherin expression, a marker of EMT (Fig. 4C), suggesting that EMT occurs downstream of FAK signaling. Altogether, our results suggest that dCol causes reduced stiffness, migration and EMT via inhibition of the FAK signaling pathway (Fig. 4D).

4. Discussion

The advance of tumor ablation treatments via destruction of local cancer tissue by thermal, mechanical, electrical and high intensity focused ultrasound have shown to selectively kill cancer cells in a target area (Takaki et al., 2017). Now, we aimed to assess the use of thermal ablation in an effort to give more evidence on selective cancer activity in

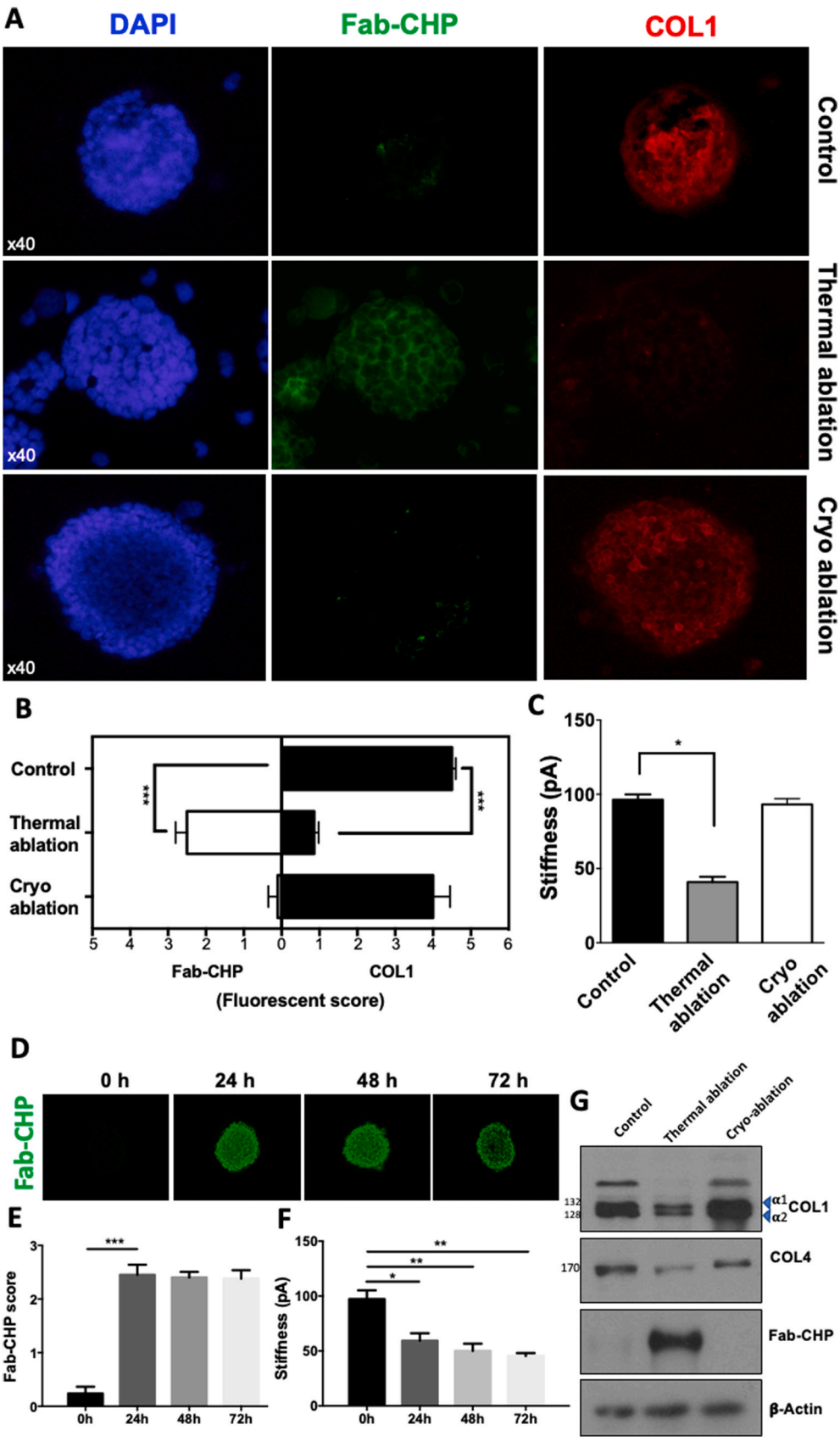

Fig. 1. Effect of thermal ablation on dCol in SK-N-DZ spheres. Representative fluorescence images shows dCol stained by Fab-CHP (green), native collagen referred by Collagen I (red), and nuclei counter stain DAPI (blue) in untreated (control; top panel), thermal ablation treatment (central panel), and cryo-ablation treatment (bottom panel) of NB spheres (A). Microscopy magnification 40X. Bar chart of Collagen 1 or Fab-CHP fluorescent score in control, thermal ablation treatment group, and cryo-ablation treatment group. The experiment was examined in triplicate with 6–7 different NB spheres (B). Bar chart shows quantification of the stiffness (pA) in control, thermal ablation treatment, and cryo-ablation treatment (C). The fluorescence of Fab-CHP was scored following 0–72 h (D). Bar charts shows the Fab-CHP score (E) and stiffness over 72 h (F). COL1, COL4, and Fab-CHP expression were examined by immunoblot (G). All asterisks denote significant changes * $P \leq 0.05$, ** $P \leq 0.001$, *** $P \leq 0.001$. Error bars indicate ± SEM.

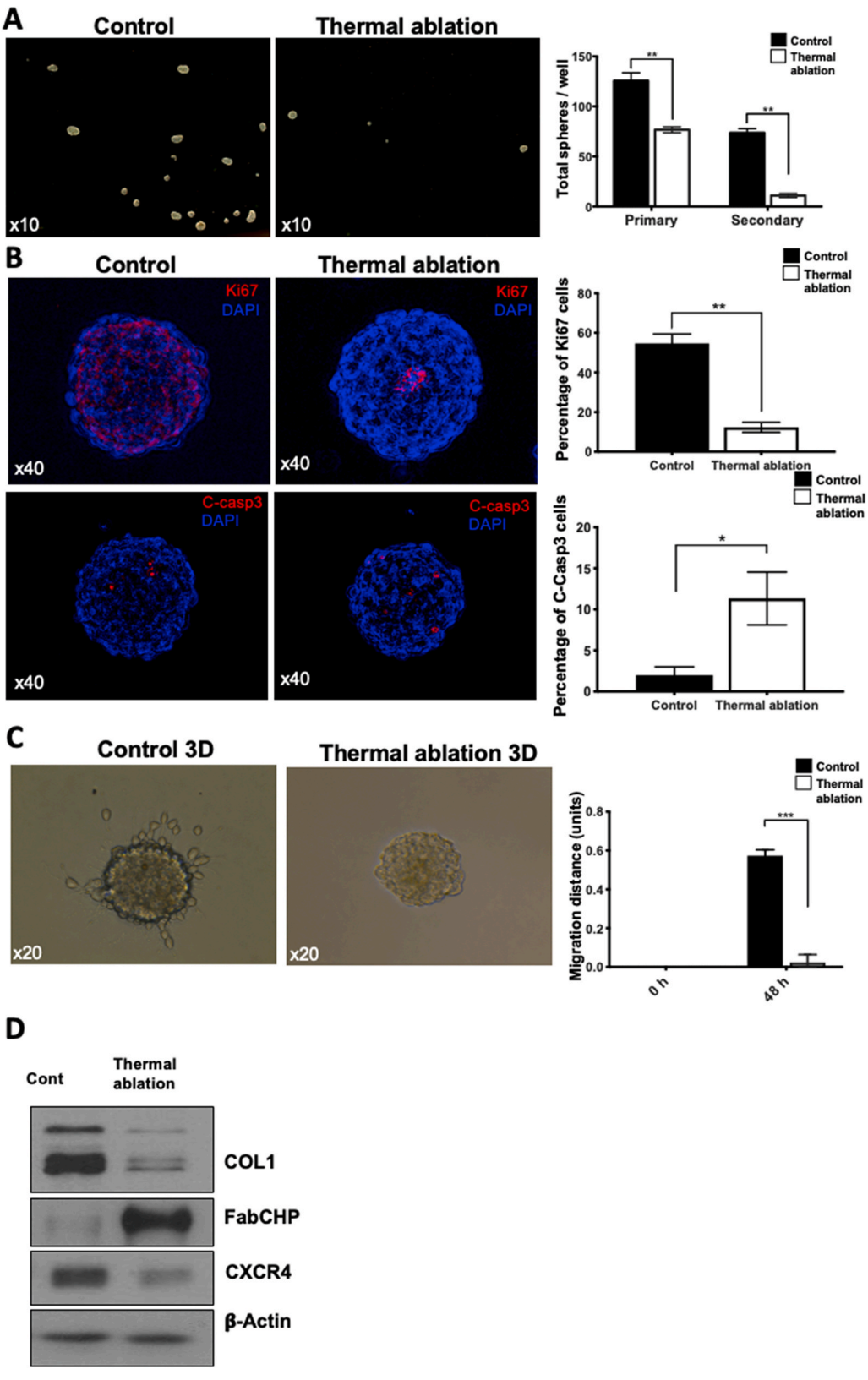

Fig. 2. dCol affects on proliferation, apoptosis, stiffness and migration of SK-N-DZ spheres. Representative image of NB sphere numbers following thermal ablation and quantified in bar charts showing sphere/well of control and thermal ablation treated groups.. Microscopy magnification 10X (A). Representative images of NB sphere fluorescent microscopy shows the proliferative marker (Ki67, red), apoptotic markers (cleavaged caspase 3, red) and nuclei-counter staining marker DAPI (blue). Microscopy magnification 40X. Quantification of staining in bar charts (right) comparing control and thermal ablation groups (B). 3D sphere migration assay comparing migration distance (units) in control and thermal ablation-treated groups at 0 and 48 hours. Bar chart on the right panel shows quantification of migration distance of 200 spheres per sample (C) (C). Immunoblot shows expression of Collagen 1, FabCHP, and CXCR4 at 48 h of wound closure between control and thermal ablation treated groups (D). All asterisks denote significant changes * $P \leq 0.05$, ** $P \leq 0.01$, ***$P \leq 0.001$. Error bars indicate ± SEM.

TME. This study is the first to reveal that thermal ablation leads to dCol and inhibition of proliferation, stiffness and migration in an NB tumor-sphere model. Furthermore, we demonstrate a role for the LOX1/LOXL2-FAK axis in this process thus providing a detailed mechanism for the inhibition of NB development by thermal ablation.

Until now, the use of either thermal or cryo-ablation for cancer treatment remains an active area of research (Shiina et al., 2018; Zhu and Rhim, 2019). Thermal ablation employs heat to directly destroy targeted tissue and can be performed using various wavelengths. This study is the first to investigate the use of thermal ablation to denature

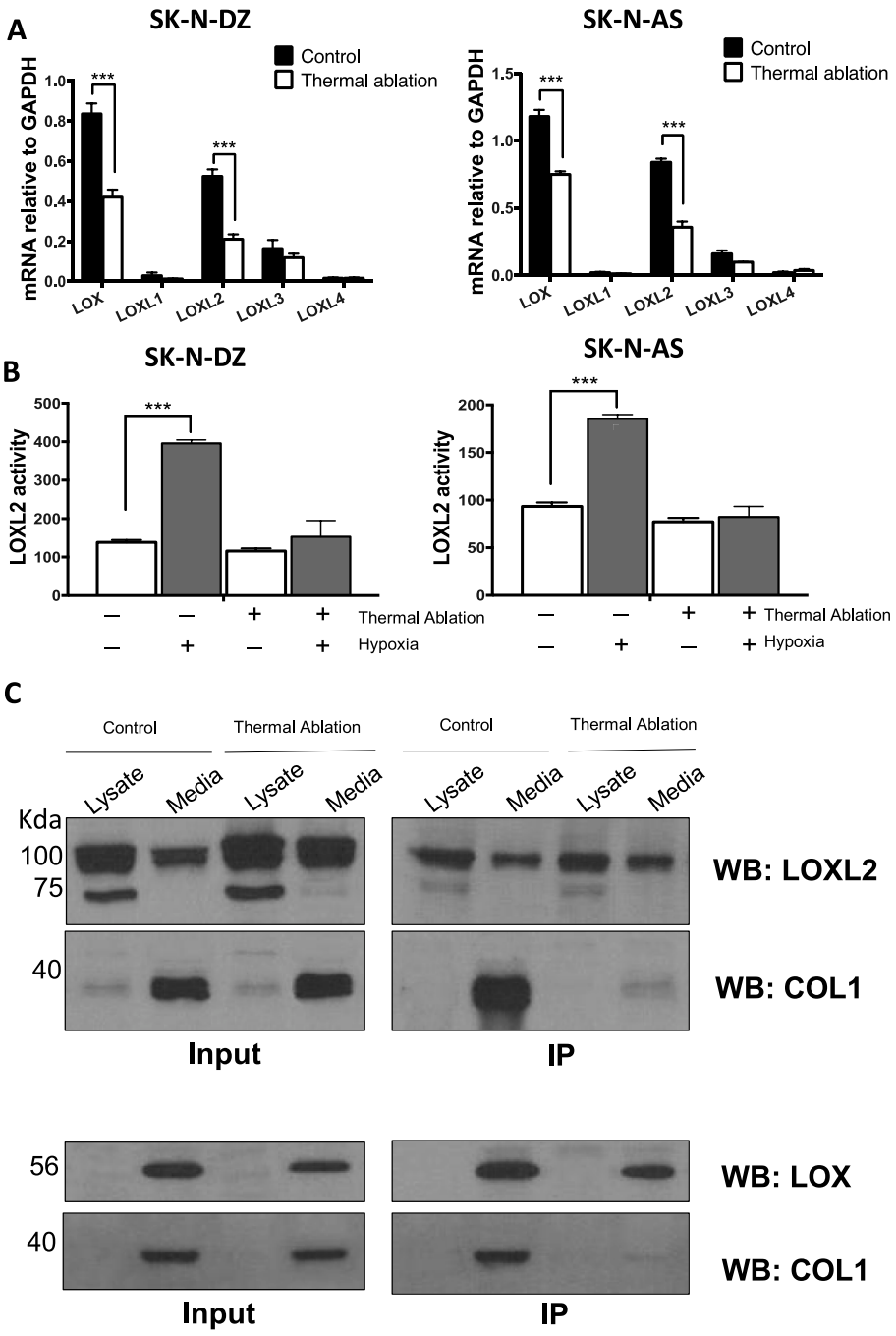

Fig. 3. Effect of dCol on LOX/LOXL2 crosslinking with type I collagen Bar charts showing mRNA levels of *LOX*, *LOXL1*, *LOXL2*, *LOXL3*, and *LOXL4* normalised to GAPDH mRNA from control and thermal ablation treatment groups for SK-N-DZ and SK-N-AS cell lines (A). Bar charts showing the LOXL2 activity under hypoxia in control and thermal ablation treated cells (B). Immunoblots show input and co-immunoprecipitation of anti-LOXL2 (upper panel), LOX (lower panel) and COL1 (upper and lower panels) from control and thermal ablation treated cells (C). All asterisks denote significant changes * $P \leq 0.05$, **$P \leq 0.001$, ***$P \leq 0.001$. Error bars indicate ± SEM.

collagen matrix in cancer cells in vitro. However, it was found to be less effective for cryo-ablation targeting collagen denaturation, likely due to deep lesions and the use of an inappropriate probe. Further studies are necessary to determine optimal protocols for cryo-ablation.

The LOX family proteins have a demonstrated role in TME remodeling that leads the process of cancer metastasis (Setargew et al., 2021). High level of either intracellular or extracellular LOX/LOXL2 expression links to reverse prognosis of various cancers (Miller et al., 2015; Peinado et al., 2008; Tanaka et al., 2018). Moreover, LOX/LOXL2 mechanistically regulates FAK signaling and contributes to EMT (Amendola et al., 2019), thus a therapy targeting LOX mediated collagen cross-linking could be promising in the treatment of solid tumors (Setargew et al., 2021). In support of previous reports (Ida et al., 2018), we found that dCol attenuates the interaction between type I collagen and extracellular LOX and/or LOXL2, and reduces LOX/LOXL2 expression. LOX/LOXL2 expression is also correlated with poor cancer survival via FAK signaling (Baker et al., 2013) and EMT phenotype (Park et al., 2017). An inhibitory effect of FAK in invasion, migration and metastasis of NB has been previously described (Barker et al., 2013; Megison et al., 2013) and, in our studies, dCol downregulated expression of phosphorylated FAK, CDC42 and EMT markers. Together these results indicate an inhibitory effect of dCol that targets the LOX/LOXL2 – FAK – EMT axis.

The inhibition of integrins and their downstream signaling pathways has been explored through the use of integrin-blocking antibodies or small molecule inhibitors targeting FAK or MAPK(Chen et al., 2022). While the role of integrins in focal-adhesion kinase and their connection with LOX/LOXL2 are important, we acknowledge that our study did not explore novel integrins and collagen crosslinking within its scope. Future studies utilizing knockdown systems targeting specific collagen types may provide further insights into potential receptors that link to

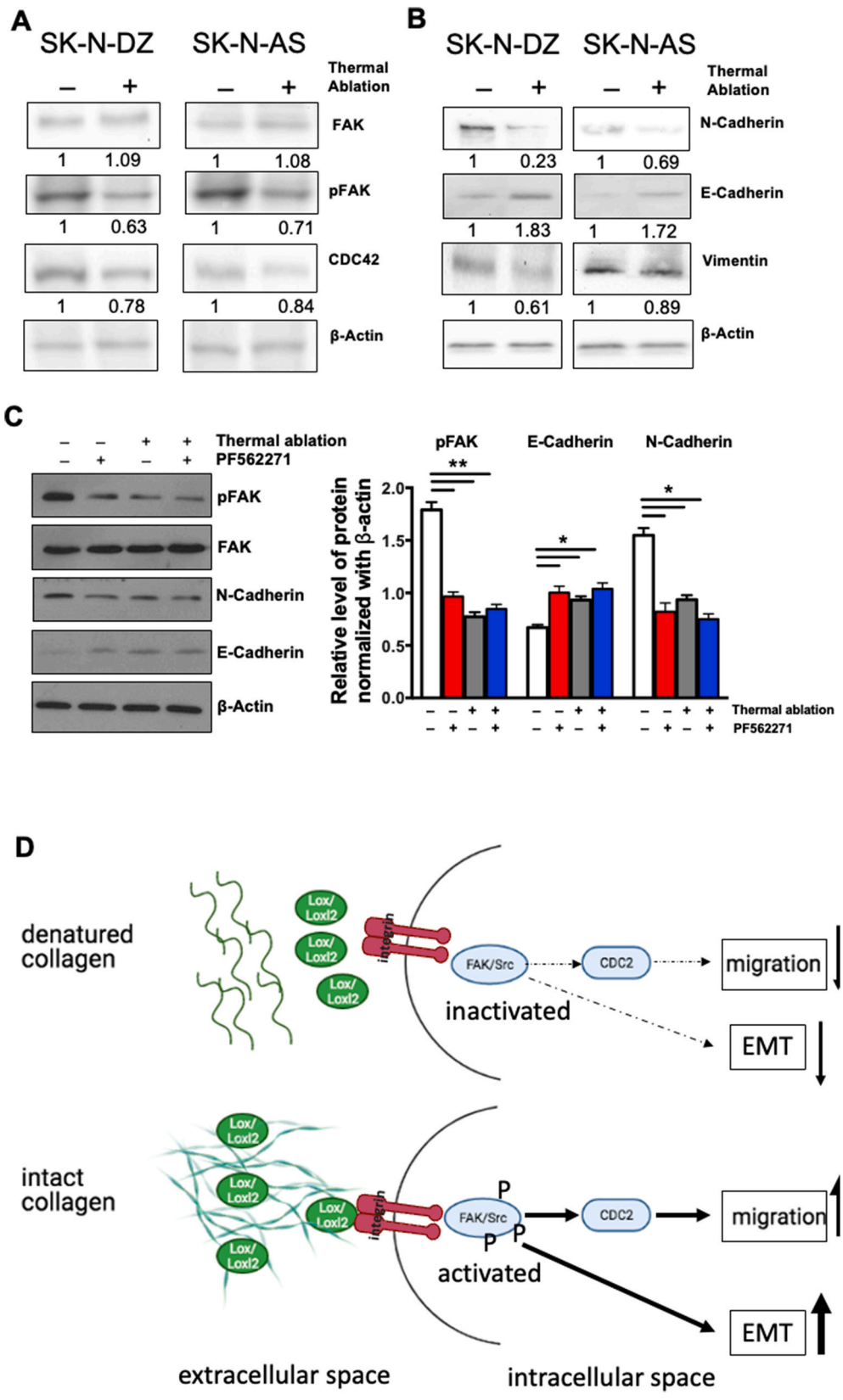

Fig. 4. Effects of dCol on FAK pathway signaling pathway and EM. Immunoblot of FAK, pFAK, and CDC42 expression showing FAK signaling comparison between control and thermal ablation treated groups (SK–N-DZ and SK-N-AS cell lines). Densitometry score is normalised to beta-actin expression in all samples (A). Immunoblot of N-Cadherin, E-Cadherin, and Vimentin expression between control and thermal ablation treated groups (SK–N-DZ and SK-N-AS cell lines). Densitometry score is normalised to beta-actin expression in all samples. Observation is examined in two different cell lines SK-N-DZ and SK-N-AS (B). Immunoblot of FAK, pFAK, N-Cadherin, and E-Cadherin protein expression between control and thermal ablation treated groups with FAK inhibitor (PF562271; C). Changes in protein levels after normalization to beta-actin are shown in the right panel bar graphs. These experiments were independently triplicated and similar results were obtained. All asterisks denote significant changes * $P \leq 0.05$, **$P \leq 0.001$. Error bars indicate ± SEM (C). Proposed mechanism of collagen denaturation impact on migration and EMT changes via the LOX/LOXL2 – FAK signaling pathway (D).

LOX/LOXL2-dependent collagen remodeling. In our study, we investigated the therapeutic approach of utilizing dCol to inhibit neuroblastoma migration and suppress epithelial-mesenchymal transition (EMT) progression. Promising preclinical and clinical studies aimed at reducing neuroblastoma cell migration and improving clinical outcomes may involve further investigation of denatured collagen through approaches such as thermal ablation, targeting integrins, or their signaling pathways.

It is important to acknowledge that our study focused solely on the effects of collagen denaturation in neuroblastoma cells, and the results may not necessarily extrapolate to other tissues or cancer models. Further studies may be needed to assess the safety and efficacy of thermal ablation in different contexts, such as skin or tendons, and consider potential effects on other tissues. While our study showed promising results *in vitro*, it is important to acknowledge that findings from cell culture experiments may not fully translate to *in vivo* settings. Therefore, further studies using animal models of NB are needed to validate the findings in a more clinically relevant setting.

This study suggests that dCol is a plausible target in the prognosis and therapy of NB. Further work is also required to better understand the complex interplay of collagen with ECM, cancer-associated fibroblasts, infiltrated immune cells and/or pro-inflammatory cytokines to establish optimal therapies for NB and potentially other solid tumor cancers.

CRediT STATEMENTS

Bao Chi Bui: Conceptualization, Methodology, Investigation, Writing - Original Draft, Writing - Review & Editing, Visualization, Supervision.

Kha Dong To: Conceptualization, Methodology, Investigation, Writing - Original Draft, Writing - Review & Editing, Supervision.

Diem My Vu: Investigation, Data Curation.

Quynh-Giang Nguyen: Investigation, Writing - Review & Editing.

Hiep Thi Nguyen: Investigation, Data Curation.

Corresponding author - Bảo Sĩ Nguyễn, Ph. D: Conceptualization, Methodology, Investigation, Writing - Original Draft, Writing - Review & Editing, Supervision, Funding acquisition.

Declaration of competing interest

The authors declare that they have no known competing financial interests or personal relationships that could have appeared to influence the work reported in this paper.

Acknowledgements

We would like to thank Dr. Izumi Hideki, Li Yuanyuan, and Michio Yasunami at Saga Medical Centre Koseikan, Japan for supplying the protocols and NB cell lines. We also thank Dr. Leigh Ann Jones of ImmunoTechniques for assistance in preparing the manuscript. The study is mainly supported by the Vietnam National University Ho Chi Minh city (#C2022-44-13).

Appendix A. Supplementary data

Supplementary data to this article can be found online at https://doi.org/10.1016/j.jtherbio.2023.103624.

References

Ahmed, A.A., Zhang, L., Reddivalla, N., Hetherington, M., 2017. Neuroblastoma in children: update on clinicopathologic and genetic prognostic factors. Pediatr. Hematol. Oncol. 34, 165–185.

Amendola, P.G., Reuten, R., Erler, J.T., 2019. Interplay between LOX enzymes and integrins in the tumor microenvironment. Cancers 11.

Baker, A.M., Bird, D., Lang, G., Cox, T.R., Erler, J.T., 2013. Lysyl oxidase enzymatic function increases stiffness to drive colorectal cancer progression through FAK. Oncogene 32, 1863–1868.

Barker, H.E., Bird, D., Lang, G., Erler, J.T., 2013. Tumor-secreted LOXL2 activates fibroblasts through FAK signaling. Mol. Cancer Res. 11, 1425.

Binnewies, M., Roberts, E.W., Kersten, K., Chan, V., Fearon, D.F., Merad, M., Coussens, L. M., Gabrilovich, D.I., Ostrand-Rosenberg, S., Hedrick, C.C., Vonderheide, R.H., Pittet, M.J., Jain, R.K., Zou, W., Howcroft, T.K., Woodhouse, E.C., Weinberg, R.A., Krummel, M.F., 2018. Understanding the tumor immune microenvironment (TIME) for effective therapy. Nat. Med. 24, 541–550.

Brock, R.M., Beitel-White, N., Davalos, R.V., Allen, I.C., 2020. Starting a fire without flame: the induction of cell death and inflammation in electroporation-based tumor ablation strategies. Front. Oncol. 10.

Brooks, M., Mo, Q., Krasnow, R., Ho, P.L., Lee, Y.C., Xiao, J., Kurtova, A., Lerner, S., Godoy, G., Jian, W., Castro, P., Chen, F., Rowley, D., Ittmann, M., Chan, K.S., 2016. Positive association of collagen type I with non-muscle invasive bladder cancer progression. Oncotarget 7, 82609–82619.

Bui, C.-B., Le, H.K., Vu, D.M., Truong, K.-D.D., Nguyen, N.M., Ho, M.A.N., Truong, D.Q., 2019. ARID1A-SIN3A drives retinoic acid-induced neuroblastoma differentiation by transcriptional repression of TERT. Mol. Carcinog. 0.

Chen, J.-R., Zhao, J.-T., Xie, Z.-Z., 2022. Integrin-mediated cancer progression as a specific target in clinical therapy. Biomed. Pharmacother. 155, 113745.

Chu, K.F., Dupuy, D.E., 2014. Thermal ablation of tumours: biological mechanisms and advances in therapy. Nat. Rev. Cancer 14, 199–208.

de Jong, O.G., van der Waals, L.M., Kools, F.R.W., Verhaar, M.C., van Balkom, B.W.M., 2019. Lysyl oxidase-like 2 is a regulator of angiogenesis through modulation of endothelial-to-mesenchymal transition. J. Cell. Physiol. 234, 10260–10269.

Franco-Luzon, L., Garcia-Mulero, S., Sanz-Pamplona, R., Melen, G., Ruano, D., Lassaletta, A., Madero, L., Gonzalez-Murillo, A., Ramirez, M., 2020. Genetic and immune changes associated with disease progression under the pressure of oncolytic therapy in A neuroblastoma outlier patient. Cancers 12.

Hanahan, D., Weinberg, R.A., 2011. Hallmarks of cancer: the next generation. Cell 144, 646–674.

Ida, T., Kaku, M., Kitami, M., Terajima, M., Rosales Rocabado, J.M., Akiba, Y., Nagasawa, M., Yamauchi, M., Uoshima, K., 2018. Extracellular matrix with defective collagen cross-linking affects the differentiation of bone cells. PLoS One 13, e0204306.

Izumi, H., Kaneko, Y., 2014. Trim32 facilitates degradation of MYCN on spindle poles and induces asymmetric cell division in human neuroblastoma cells. Cancer Res. 74, 5620–5630.

Joshi, S., 2020. Targeting the tumor microenvironment in neuroblastoma: recent advances and future directions. Cancers 12, 1–22.

Li, Y., Foss, C.A., Summerfield, D.D., Doyle, J.J., Torok, C.M., Dietz, H.C., Pomper, M.G., Yu, S.M., 2012. Targeting collagen strands by photo-triggered triple-helix hybridization. Proc. Natl. Acad. Sci. U. S. A 109, 14767–14772.

Liu, B., Zhou, L., Huang, G., Zhong, Z., Jiang, C., Shan, Q., Xu, M., Kuang, M., Xie, X., 2015. First experience of ultrasound-guided percutaneous ablation for recurrent hepatoblastoma after liver resection in children. Sci. Rep. 5, 16805-16805.

Lu, P., Weaver, V.M., Werb, Z., 2012. The extracellular matrix: a dynamic niche in cancer progression. JCB (J. Cell Biol.) 196, 395–406.

Mazouni, C., Arun, B., André, F., Ayers, M., Krishnamurthy, S., Wang, B., Hortobagyi, G. N., Buzdar, A.U., Pusztai, L., 2008. Collagen IV levels are elevated in the serum of patients with primary breast cancer compared to healthy volunteers. Br. J. Cancer. 99, 68–71.

Megison, M.L., Stewart, J.E., Nabers, H.C., Gillory, L.A., Beierle, E.A., 2013. FAK inhibition decreases cell invasion, migration and metastasis in MYCN amplified neuroblastoma. Clin. Exp. Metastasis 30, 555–568.

Miles, C.A., Ghelashvili, M., 1999. Polymer-in-a-box mechanism for the thermal stabilization of collagen molecules in fibers. Biophys. J. 76, 3243–3252.

Miller, B.W., Morton, J.P., Pinese, M., Saturno, G., Jamieson, N.B., McGhee, E., Timpson, P., Leach, J., McGarry, L., Shanks, E., Bailey, P., Chang, D., Oien, K., Karim, S., Au, A., Steele, C., Carter, C.R., McKay, C., Anderson, K., Evans, T.R.J., Marais, R., Springer, C., Biankin, A., Erler, J.T., Sansom, O.J., 2015. Targeting the LOX/hypoxia axis reverses many of the features that make pancreatic cancer deadly: inhibition of LOX abrogates metastasis and enhances drug efficacy. EMBO Mol. Med. 7, 1063–1076.

Okada, K., Moon, H.-J., Finney, J., Meier, A., Mure, M., 2018. Extracellular processing of lysyl oxidase-like 2 and its effect on amine oxidase activity. Biochemistry 57, 6973–6983.

Park, P.-G., Jo, S.J., Kim, M.J., Kim, H.J., Lee, J.H., Park, C.K., Kim, H., Lee, K.Y., Kim, H., Park, J.H., Dong, S.M., Lee, J.M., 2017. Role of LOXL2 in the epithelial-mesenchymal transition and colorectal cancer metastasis. Oncotarget 8, 80325–80335.

Pavlovich, C.P., Walther, M.M., Choyke, P.L., Pautler, S.E., Chang, R., Linehan, W.M., Wood, B.J., 2002. Percutaneous radio frequency ablation of small renal tumors: initial results. J. Urol. 167, 10–15.

Peinado, H., Moreno-Bueno, G., Hardisson, D., Pérez-Gómez, E., Santos, V., Mendiola, M., de Diego, J.I., Nistal, M., Quintanilla, M., Portillo, F., Cano, A., 2008. Lysyl oxidase–like 2 as a new poor prognosis marker of squamous cell carcinomas. Cancer Res. 68, 4541.

Pinto, N.R., Applebaum, M.A., Volchenboum, S.L., Matthay, K.K., London, W.B., Ambros, P.F., Nakagawara, A., Berthold, F., Schleiermacher, G., Park, J.R., Valteau-Couanet, D., Pearson, A.D., Cohn, S.L., 2015. Advances in risk classification and treatment strategies for neuroblastoma. J. Clin. Oncol. 33, 3008–3017.

Rhim, H., Yoon, K.H., Lee, J.M., Cho, Y., Cho, J.S., Kim, S.H., Lee, W.J., Lim, H.K., Nam, G.J., Han, S.S., Kim, Y.H., Park, C.M., Kim, P.N., Byun, J.Y., 2003. Major complications after radio-frequency thermal ablation of hepatic tumors: spectrum of imaging findings. Radiographics 23, 123–134.

Ricard-Blum, S., 2011. The collagen family. Cold Spring Harbor Perspect. Biol. 3, a004978.

Ringel-Scaia, V.M., Beitel-White, N., Lorenzo, M.F., Brock, R.M., Huie, K.E., Coutermarsh-Ott, S., Eden, K., McDaniel, D.K., Verbridge, S.S., Rossmeisl, J.H., Oestreich, K.J., Davalos, R.V., Allen, I.C., 2019. High-frequency irreversible electroporation is an effective tumor ablation strategy that induces immunologic cell death and promotes systemic anti-tumor immunity. EBioMedicine 44, 112–125.

Roduit, C., Sekatski, S., Dietler, G., Catsicas, S., Lafont, F., Kasas, S., 2009. Stiffness tomography by atomic force microscopy. Biophys. J. 97, 674–677.

Setargew, Y.F.I., Wyllie, K., Grant, R.D., Chitty, J.L., Cox, T.R., 2021. Targeting lysyl oxidase family meditated matrix cross-linking as an anti-stromal therapy in solid tumours. Cancers 13.

Shiina, S., Sato, K., Tateishi, R., Shimizu, M., Ohama, H., Hatanaka, T., Takawa, M., Nagamatsu, H., Imai, Y., 2018. Percutaneous ablation for hepatocellular carcinoma: comparison of various ablation techniques and surgery. Canadian Journal of Gastroenterology and Hepatology 2018, 4756147.

Takaki, H., Cornelis, F., Kako, Y., Kobayashi, K., Kamikonya, N., Yamakado, K., 2017. Thermal ablation and immunomodulation: from preclinical experiments to clinical trials. Diagnostic and Interventional Imaging 98, 651–659.

Tanaka, N., Yamada, S., Sonohara, F., Suenaga, M., Hayashi, M., Takami, H., Niwa, Y., Hattori, N., Iwata, N., Kanda, M., Tanaka, C., Kobayashi, D., Nakayama, G., Koike, M., Fujiwara, M., Fujii, T., Kodera, Y., 2018. Clinical implications of lysyl oxidase-like protein 2 expression in pancreatic cancer. Sci. Rep. 8, 9846.

Truong, D.Q., Ho, B.T., Chau, G.C., Truong, D.K., Pham, T.T.T., Nakagawara, A., Bui, C. B., 2022. Collagen XI Alpha 1 (COL11A1) Expression in the Tumor Microenvironment Drives Neuroblastoma Dissemination. Pediatr. Dev. Pathol. 25, 91–98.

Xu, S., Xu, H., Wang, W., Li, S., Li, H., Li, T., Zhang, W., Yu, X., Liu, L., 2019. The role of collagen in cancer: from bench to bedside. J. Transl. Med. 17, 309.

Zhu, F., Rhim, H., 2019. Thermal ablation for hepatocellular carcinoma: what's new in 2019. Chin. Clin. Oncol. 8, 58.

Zitnay, J.L., Li, Y., Qin, Z., San, B.H., Depalle, B., Reese, S.P., Buehler, M.J., Yu, S.M., Weiss, J.A., 2017. Molecular level detection and localization of mechanical damage in collagen enabled by collagen hybridizing peptides. Nat. Commun. 8, 14913.